ChemPubSoc Europe

DOI: 10.1002/chem.201802040

CHEMISTRY A European Journal Full Paper

Oxygen Reduction Reaction | *Hot Paper*

Microporous N,P-Codoped Graphitic Nanosheets as an Efficient Electrocatalyst for Oxygen Reduction in Whole pH Range for Energy Conversion and Biosensing Dissolved Oxygen

Deqing Lin,[a, b] Chuangang Hu,[b] Hao Chen,*[a] Jia Qu,*[a] and Liming Dai*[a, b]

Abstract: Microporous N,P-codoped graphitic nanosheets (N,P-CMP-1000) were synthesized by thermal annealing (1000 °C) of as-synthesized conjugated microporous polymers (CMPs) in the presence of phytic acid, which can be used as an effective metal-free electrocatalyst for the oxygen reduction reaction (ORR) for energy conversion. In the whole pH range (i.e. alkaline, acidic, and neutral solutions), the obtained N,P-CMP-1000 exhibits superior electrocatalytic activity for ORR with a low overpotential, high current density, and good stability. Furthermore, N,P-CMP-1000 can also be applied for electrochemically sensing dissolved oxygen (DO), with a high sensitivity (1.89 $\mu A\,mg^{-1}\,L$) and broad detection range (2.56 to 16.65 $mg\,L^{-1}$) due to its good electrocatalytic performance towards ORR in neutral solution. In vitro cytotoxicity tests (CCK-8 and Live/Dead Cell Double Staining Assay) of N,P-CMP-1000 extracts demonstrated its good biocompatibility to Human Corneal Epithelial Cells (HCEC), which shows its great potential as an eye-wearable biosensor for sensing DO in tears.

Introduction

The oxygen reduction reaction (ORR) is the key process, not only in environmentally benign energy storage and conversion technologies, such as fuel cells and metal-air batteries,[1] but also in a variety of biochemical reactions and even in electrochemical biosensors for the detection of dissolved oxygen (DO).[2] In biological systems, sufficient oxygen in bodily fluid is a prerequisite to maintain normal metabolic activities. For instance, extended-wear contact lenses often lead to deficiencies of dissolved oxygen (DO) in tears and subsequent ophthalmic diseases.[3] Therefore, it is of great importance to keep real-time and in vivo monitoring of oxygen concentration in tears for contact lens wearers. Among various reported DO detection strategies, the electrochemical method offers advantages because of its high sensitivity, easy operation, and rapid response.[4] In order to fabricate high-performance energy-related devices or electrochemical DO biosensors, however, it is highly desirable to develop superior electrocatalysts for ORR in the whole pH range.

The commonly used platinum (Pt) electrocatalyst for ORR suffers from multiple drawbacks, including high cost, scarcity, fuel crossover effect, and CO poisoning, which greatly hampered its large-scale application.[5] Therefore, non-precious metal catalysts (e.g., Fe-N-C),[6] and metal-free carbon materials,[7] have been developed to replace Pt as ORR electrocatalysts. Having advantages of a low price, high electrocatalytic activity, long-term operational stability, and tolerance to fuel crossover effect and CO poisoning, vertically aligned nitrogen-doped carbon nanotubes have been demonstrated to be an excellent metal-free ORR electrocatalyst in alkaline media.[7a] Subsequently, various heteroatom-doped carbon materials, such as graphene,[8] carbon nanotubes,[9] porous carbon,[10] nanoribbon,[11] and quantum dots,[12] were reported to also exhibit good electrocatalytic performance towards ORR.[1,13] Combined experimental and theoretical studies indicated that the doping-induced charge transfer between the heteroatom and carbon atoms improved the absorption of oxygen onto the active center, which could weaken the oxygen bond to lower the overpotential for ORR. Comparing to the single-atom doping, N,B-,[14] N,S-,[10b,15] and N,P-[16] codoping was found to show superior electrocatalytic performance towards ORR through synergistic effects.[1,14] Despite their excellent ORR electrocatalytic activities in alkaline solution, the electrocatalytic performance of carbon-based metal-free electrocatalysts in acidic[17] and neutral[18] solutions needs to be further improved.

[a] D. Lin, Prof. H. Chen, Prof. J. Qu, Prof. L. Dai
Institute of Advanced Materials for Nano-Bio Applications
School of Ophthalmology & Optometry
Wenzhou Medical University
270 Xueyuan Xi Road
Wenzhou, Zhejiang 325027 (China)
E-mail: chenhao@mail.eye.ac.cn
jia.qu@163.com
l.dai@hotmail.com

[b] D. Lin, Dr. C. Hu, Prof. L. Dai
Center of Advanced Science and Engineering for Carbon (Case4Carbon)
Department of Macromolecular Science and Engineering
Case Western Reserve University
10900 Euclid Avenue
Cleveland, Ohio 44106 (USA)

Supporting information and the ORCID identification number(s) for the author(s) of this article can be found under: https://doi.org/10.1002/chem.201802040.

Part of a Special Issue focusing on topics within the field of renewable energy. To view the complete issue, visit Issue 69.

It is still quite challenging to develop carbon-based electrocatalysts for ORR in whole pH range, especially in acidic and neutral solutions.[19]

On the other hand, porous carbon catalysts with a high specific surface area (SSA) can greatly enhance the electrocatalytic capability by effectively exposing the active sites and facilitating the electrolyte transport.[20] Without involving a template,[21] porous graphitic carbons can be directly synthesized from the porous polymers derived from covalent organic polymers (COPs).[22] However, precise synthesis of designed porous polymers is still difficult, if not impossible, as they are usually synthesized under harsh conditions.[23,24] While more methods for facile and precise syntheses of porous heteroatom(s)-containing polymers are being developed, N-doped porous graphitic carbons have recently been prepared by thermal annealing of N-containing COPs as efficient metal-free ORR electrocatalysts.[23]

Herein, we report a facile synthesis of a conjugated microporous polymer (CMP) by acid-catalyzed condensation of commercially available 1,2,4,5-benzenetetramine and hexaketocyclohexane (Figure 1a) by following a reported procedure with modifications.[25] Subsequently, thermal annealing of CMP and CMP/phytic acid composite at high temperatures (e.g., 900 or 1000 °C) yielded a monodoped sample (N-CMP-900) and codoped samples (N,P-CMP-900 and N,P-CMP-1000) as porous graphitic carbon nanosheets. It is worth mentioning that no metallic chemical was involved in the whole synthesis process. Among all the resulting carbonized samples, codoped N,P-CMP-1000 exhibited the best ORR performance, not only in alkaline solution, but also in acidic and neutral solutions. The codoping, coupled with a high exposure of active sites in the porous N,P-CMP-1000, is responsible for the observed high electrocatalytic performance. Having good electrocatalytic activity for ORR in neutral solution, N,P-CMP-1000 was used to fabricate an electrochemical DO biosensor with good sensitivity and broad detection range, which is the first time that metal-free electrocatalysts based on codoped carbons have been used for DO sensing.

Results and Discussion

Unlike the high-temperature ionothermal method often used for the synthesis of *p*-conjugated microporous polymeric frameworks,[24] the acid-catalyzed condensation of 1,2,4,5-benzenetetramine and hexaketocyclohexane was applied to synthesize the desired CMP, as shown in Figure 1. Fourier transform infrared (FTIR) spectra given in Figure S1 (Supporting Information) confirmed the formation of CMP by the disappearance of two peaks assigned, respectively, to the stretching vibration of amino ($-NH_2$) and quinoyl (-C=O) group in the two reactants, with a concomitant appearance of an imine (-C=N-) stretching vibration peak for the aza-ring.[24a] Subsequent pyrolysis of the newly-formed CMP in the presence of phytic acid at 1000 °C produced the N,P-codoped graphitic nanosheets (i.e., N-CMP-1000). For comparison, N-CMP-900 with only N-doping was also prepared under the same condition, but at 900 °C in the absence of phytic acid (see Supporting Information for the detailed synthesis).

Transmission electron microscope (TEM) images of N,P-CMP-1000 under different magnifications clearly show a thin nanosheet structure and the existence of nanopores (Figure 1b, c). TEM images of CMP, N-CMP-900, and N,P-CMP-900 exhibit similar morphologies to N,P-CMP-1000 (Figure S2). The high-angle annular dark-field scanning transmission electron microscope (HAADF-STEM) image (Figure 1d) further confirmed the sheet like structure, and the corresponding HAADF-STEM mappings (Figure 1e–g) show a uniform distribution of C (red), N (orange), and P (yellow) elements over the whole nanosheet.

N_2 adsorption/desorption isotherms were measured at 77 K to evaluate their specific surface area (SSA) as before and after carbonization. Compared with the as-synthesized CMP (27 $m^2 g^{-1}$), the Brunauer–Emmett–Teller (BET) specific surface

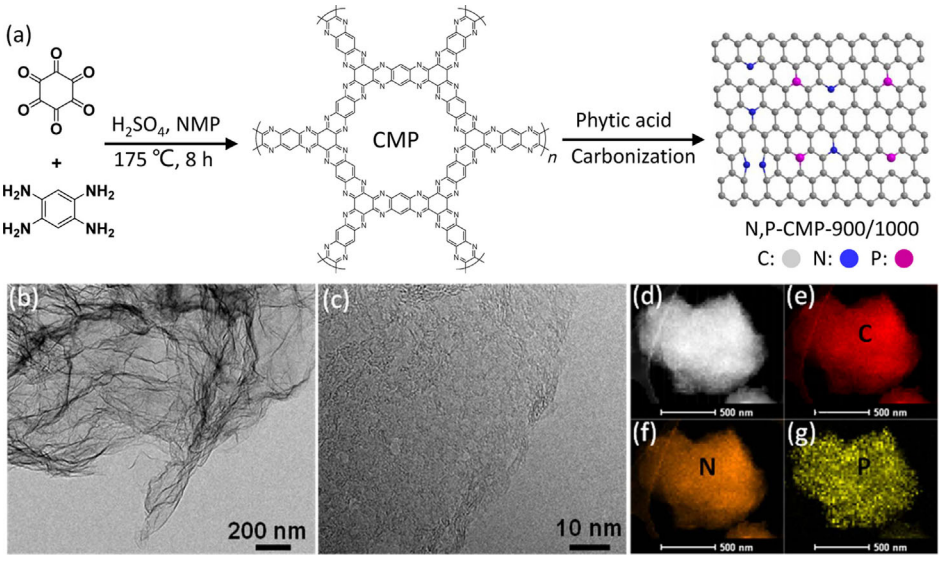

Figure 1. (a) Schematic illustration of the preparation of CMP and codoped derivatives. TEM image (b) and high-resolution TEM image (c) of N,P-CMP-1000. The STEM image (d) and element mapping images for C (e), N (f) and P (g) of N,P-CMP-1000.

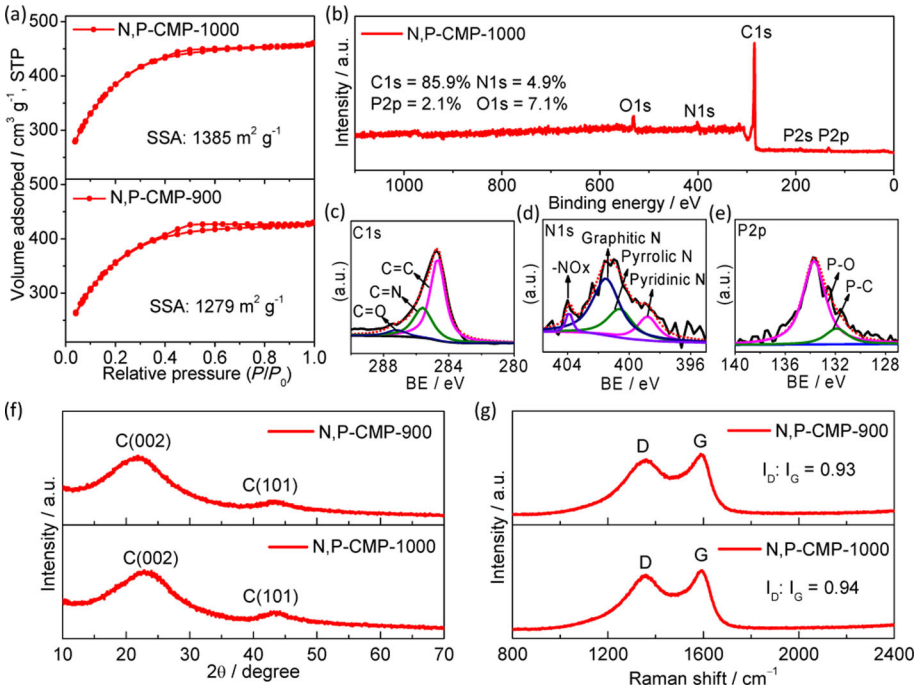

Figure 2. (a) N_2 adsorption/desorption isotherms of codoped CMPs. XPS survey spectrum (b) and high-resolution XPS spectra of C 1s (c), N 1s (d), and P 2p (e) of N,P-CMP-1000 (Note: -NOx and BE mean oxidized nitrogen and binding energy, respectively). XRD patterns (f) and Raman spectra (g) of codoped CMPs.

area of N-CMP-900 increased by several times to 171 $m^2 g^{-1}$ after pyrolysis (Figure S3). Codoping with the second heteroatom P was found to further enhance the BET specific surface area up to 1279 $m^2 g^{-1}$ for N,P-CMP-900 and 1385 $m^2 g^{-1}$ for N,P-CMP-1000 (Figure 2a). The observed ultrahigh specific surface area for the N,P-codoped samples can be attributed to the high content of oxygen in the starting materials of hexaketocyclohexane and phytic acid, to serve as a carbon-etching agent for the micropore formation during carbonization, as confirmed by the classical type I reversible N_2 sorption profiles (Figure 2a) and TEM images (Figure 1c). Both the high specific surface area and microporous structure could improve the electrocatalytic activity by exposing more active sites and facilitating electrolyte diffusion.

X-ray photoelectron spectroscopy (XPS) was performed to quantitatively measure the elemental composition of CMP and the pyrolyzed derivatives. Figure 2b shows the XPS survey spectrum of N,P-CMP-1000, which reveals characteristic peaks of C, N, and P arising from the codoping of a graphitic carbon skeleton with N and P.[10a] The presence of the O peak in Figure 2b indicates oxygen residues from starting materials of hexaketocyclohexane and phytic acid in the final carbon nanosheets, though the presence of some physically absorbed O_2 molecules cannot be ruled out.[14b] High-resolution XPS spectra of C 1s (Figure 2c), N 1s (Figure 2d) and P 2p (Figure 2e) were also measured. After deconvolution, the XPS C 1s spectrum exhibits two main peaks ascribed to graphitic carbon (C=C) and N-bonded carbon (C=N), indicating the successful doping of N into the carbonized N,P-CMP-1000. The XPS N 1s spectrum (Figure 2d) can be deconvoluted into four different species of N, which are pyridinic (398.8 eV), pyrrolic (400.6 eV), graphitic (401.5 eV), and oxidized nitrogen (403.9 eV), respectively. The high-resolution XPS P 2p spectrum can be deconvoluted into two main P species, P–O (133.7 eV) and P–C (131.9 eV), which further confirmed the successful incorporation of P into the graphitic carbon skeleton. Similarly, the XPS survey spectra of CMP, N-CMP-900 and N,P-CMP-900 show the desired elemental composition, without any obvious impurity contamination (Figure S4).

As shown in XRD profiles (Figure 2f and Figure S5 in Supporting Information), both N-CMP and N,P-CMP exhibited two characteristic graphitic (002) and (101) diffraction peaks, centered at 26.4 and 43.6°, respectively. Compared to N-CMP, the (002) peak of N,P-CMP-900 or N,P-CMP-1000 shifted to a smaller angle with an increased interlayer distance, indicating the doping of the relatively big P atoms into the carbon network. We further performed Raman spectroscopy. As shown in Figure 2g and Figure S6, both N-CMP and N,P-CMP exhibited two characteristic D and G peaks centered at 1358 and 1590 cm^{-1}, respectively. The enhanced I_D:I_G ratios for pyrolyzed samples could be attributed to the heteroatom doping induced disorder, and edge defects associated with the pores within the porous carbon frameworks. Thus, the resultant N,P-CMPs with a high surface area, good porosity, and reasonable graphitization degree should be attractive as metal-free electrocatalysts for ORR.

To investigate the electrocatalytic properties, we first performed cyclic voltammetric (CV) measurements on carbonized CMPs towards ORR in 0.1 M KOH solution. As can be seen in Figure 3a, oxygen reduction peaks are clearly seen for N,P-CMP-1000 in an O_2-saturated solution, but not in a N_2-saturated solution (cf., Figure S7). A more positive ORR peak was ob-

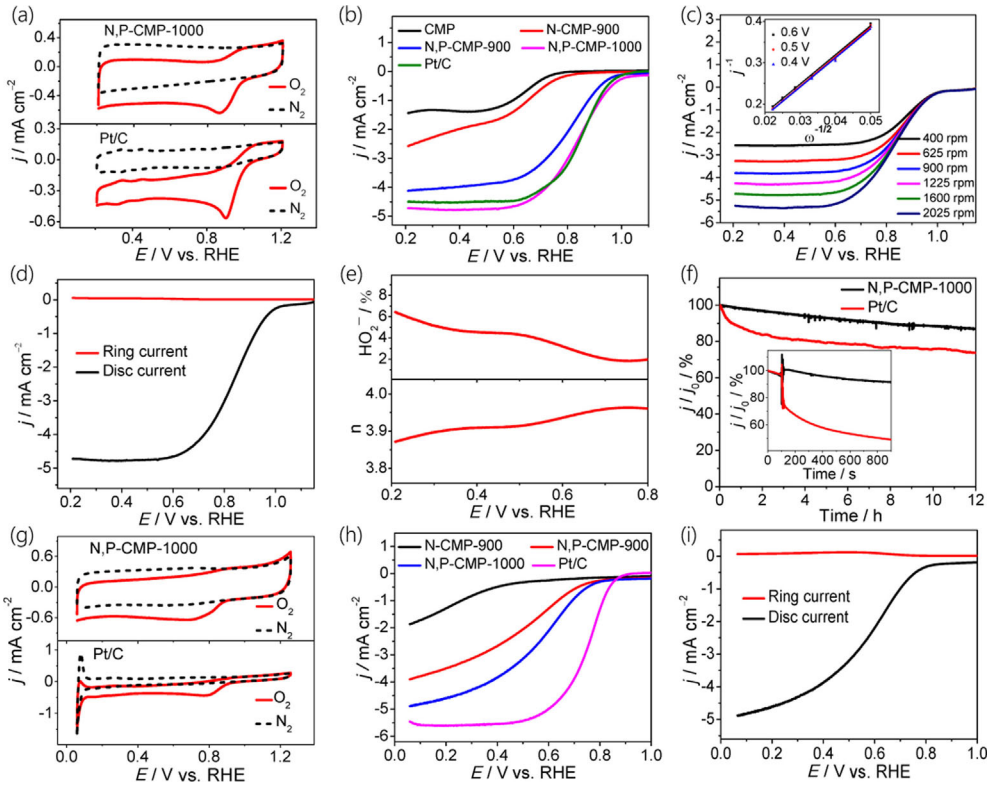

Figure 3. Electrocatalytic activity for ORR in 0.1 M KOH (a–f) and 0.1 M $HClO_4$ (g–i) solutions. (a) CV curves of N,P-CMP-1000 and commercial Pt/C electrocatalysts in KOH solutions saturated with O_2 or N_2. (b) LSV curves of different samples at 1600 rpm rotating speed on RDE. (c) LSV curves of N,P-CMP-1000 at different rotating speeds (Inset: *K-L* plots for N,P-CMP-1000 at different potentials). (d) RRDE measurement for N,P-CMP-1000 at 1600 rpm rotating speed. (e) Percentage of HO_2^- in the total oxygen reduction products and the electron transfer number per oxygen (*n*) of N,P-CMP-1000 based on the RRDE measurements. (f) Stability test and methanol (3 M) crossover effect test (Inset image) of N,P-CMP-1000 (black) and Pt/C (red) at 1600 rpm rotating speed. (g) CV curves of N,P-CMP-1000 and commercial Pt/C in a $HClO_4$ (0.1 M) solution saturated with O_2 or N_2, (h) LSV curves of different samples at 1600 rpm rotating speed on RDE in a $HClO_4$ (0.1 M) solution. (i) RRDE measurement for N,P-CMP-1000 at 1600 rpm rotating speed in a $HClO_4$ (0.1 M) solution.

served for codoped N, P-CMP-1000 (0.86 V vs. the reversible hydrogen electrode, RHE) in respect to monodoped N-CMP-900 (0.66 V), and N,P-CMP-900 (0.85 V), which is comparable to the commercial state-of-art ORR electrocatalyst of Pt/C (0.90 V vs. RHE).

Linear sweep voltammetry (LSV) measurements were also conducted on a rotating disk electrode (RDE) to further determine the electrocatalytic activity of doped CMPs towards O_2 reduction. Among all the metal-free catalysts investigated in this study, N,P-CMP-1000 exhibited the best electrocatalytic activity, with a positive onset potential of 0.94 V and a half-wave potential of 0.84 V at the rotating speed of 1600 rpm, which are very close values to those of commercial Pt/C (0.95 V, 0.85 V) (Figure 3b). Compared to Pt/C, N,P-CMP-1000 shows an even higher diffusion-limiting current density (Figure 3b). The LSV curves under different rotating speeds were measured to determine the electron transfer number per oxygen molecule (*n*) and kinetic current density (j_K) by the Koutechy–Levich (*K-L*) equation (Figure 3c and Figure S8). As can be seen the inset in Figure 3c, a linear relationship between j^{-1} and $\omega^{-1/2}$ (*K-L* plots) was obtained for N,P-CMP-1000, and, from its slope and intercept, the *n* and kinetic current density (j_k) were calculated to be >3.96 and 27 mA cm^{-2} at 0.6 V, respectively, outperforming most reported metal-free electrocatalysts for ORR.[1a]

A rotating ring disk electrode (RRDE) was also applied to determine the *n* value and the percentage of peroxide species (HO_2^-%). From Figure 3d and the equations given in the Electrochemical Test section in the Supporting Information, the hydrogen peroxide yield was calculated to be <6% and *n* to be >3.9 for N,P-CMP-1000 under a large potential range of 0.2 to 0.8 V (Figure 3e), which is in good agreement with the *n* value calculated from *K-L* equation. Furthermore, compared with Pt/C, N,P-CMP-1000 further exhibited a better stability with less attenuation of current density over 12 h, and almost no methanol cross-over effect (Figure 3f).

These results indicate N,P-CMP-1000 exhibited an excellent electrocatalytic activity for ORR in alkaline solution by an effective four-electron process. The ORR electrocatalytic activity of codoped N,P-CMP-1000 in 0.1 M $HClO_4$ solution was also tested. As shown in Figure 3g, codoped N,P-CMP-1000 exhibited an obvious oxygen reduction peak at 0.68 V in O_2-saturated 0.1 M $HClO_4$ solution, indicating a reasonably high electrocatalytic activity for ORR in acidic conditions. The corresponding LSV curves are given in Figure 3h and Figure S9a, which show a good ORR activity for N,P-CMP-1000 with a positive onset potential of 0.75 V and a half-wave potential of 0.57 V at the rotating speed of 1600 rpm. From the RRDE results in Figure 3i, the electron transfer number per oxygen molecule (*n*)

and hydrogen peroxide (H_2O_2) percentage in the total oxygen reduction products were also calculated to be >3.5 and $<20\%$, respectively, for N,P-CMP-1000 over the potential range of 0.2–0.5 V, which is in accordance with an *n* value of 3.5 at 0.5 V, derived from the *K-L* plots (Figure S9 b,c). These CV and LSV results from N,P-CMP-1000 indicate good ORR performance with a four-electron process in acidic solution, comparable to the reported non-precious Fe-N/C-800[26] and N,S-G.[27]

Similarly, good ORR electrocatalytic activities were observed for N,P-CMP-1000 in neutral electrolyte (PBS solution, Figure 4 a–c, Figures S10 and S11). More specifically, N,P-CMP-1000 exhibited a CV with a positive ORR peak potential (0.53 V), comparable to that of the commercial Pt/C (0.60 V) (Figure S10). The LSV curve of N,P-CMP-1000 in Figure S11 a shows a positive half-wave potential of 0.48 V at the rotating speed of 1600 rpm, which is also close to that of Pt/C (0.58 V). As shown in Figure 4 a–c, *n* values calculated from the *K-L* plots (Figure 4 a) and the RRDE results (Figure 4 b) are both equal to ≈ 3.8, whereas the percentage of H_2O_2 in total oxygen reduction products is below 12% over the potential range of 0.1–0.5 V (Figure 4 c). Under continuous operation for 2 h in an O_2-saturated PBS solution, N,P-CMP-1000 showed a good stability with only 15% decrease in the limiting current (Figure S11 b). These results proved that N,P-CMP-1000 can reduce oxygen through a four-electron process mainly into water, not toxic hydrogen peroxide, which should facilitate in vivo monitoring of DO in body fluid without causing apparent damage to living tissues.

So far, most electrochemical DO biosensors were reported to utilize precious metals (Pt[28] and Au[29]) or non-precious metals (Fe[30] and Co[2]) as electrocatalysts, which are expensive and toxic to tissues. Therefore, nontoxic and metal-free carbon electrocatalysts are very attractive for the fabrication of wearable electrochemical DO biosensors. In this study, therefore, we used for the first time, codoped carbon nanosheets (N,P-CMP-1000) as a metal-free ORR catalyst in electrochemical DO biosensors and evaluated its electrocatalytic performance. As shown in Figure 4 d, the cathodic current (I_c) at the N,P-CMP-1000 modified glassy carbon electrode (GCE) increased linearly with increasing the concentration of dissolved oxygen (DO) in the PBS solution. The cathodic peak currents (I_{cp}) of different DO solutions can be obtained from LSV curves of corresponding PBS solutions (seeing the Electrochemical Test section and Figure S12 in the Supporting Information). Figure 4 e shows the calibration plot of cathodic peak current (I_{cp}) versus DO concentration (C_{DO}) with a linear relationship in the concentration range of 2.56 to 16.65 mg L^{-1}, which covers the DO concentration variation in naturally air-saturated water (≈ 9 mg L^{-1} at 20 °C) and human tears. This calibration plot can be fitted by a linear equation: $I_{cp} = 1.89 * C_{DO}$ (mg L^{-1}) + 0.48 with a correlation coefficient (R^2) of 0.992. From this linear equation, the sensitivity of our electrochemical DO sensor based on N,P-CMP-1000 is found to be 1.89 μA mg^{-1} L or 26.62 μA mg^{-1} L cm^{-2}. To approve its application in clinical tests, DO concentrations in air-saturated PBS solution and commercial artificial tears were determined to be 9.53 and 9.74 mg L^{-1}, respectively, using a N,P-CMP-1000 modified GCE and with the calibration equation (Figure 4 f). By comparing with the results of C_{DO} (9.72 and 9.81 mg L^{-1}) tested by a commercial DO biosensor (inset images of Figure 4 f, Figure S12), it can be seen that the electrochemical DO sensor constructed from N,P-CMP-1000 in this work shows great performance with $<3\%$ deviation. Furthermore, the low charge-transfer resistance seen in Figure S13 for N,P-CMP-1000 could ensure a fast and sensitive response for DO sensors based on N,P-CMP-1000.

For the potential application in eye-wearable biosensors to determine DO, it is necessary and important to evaluate the

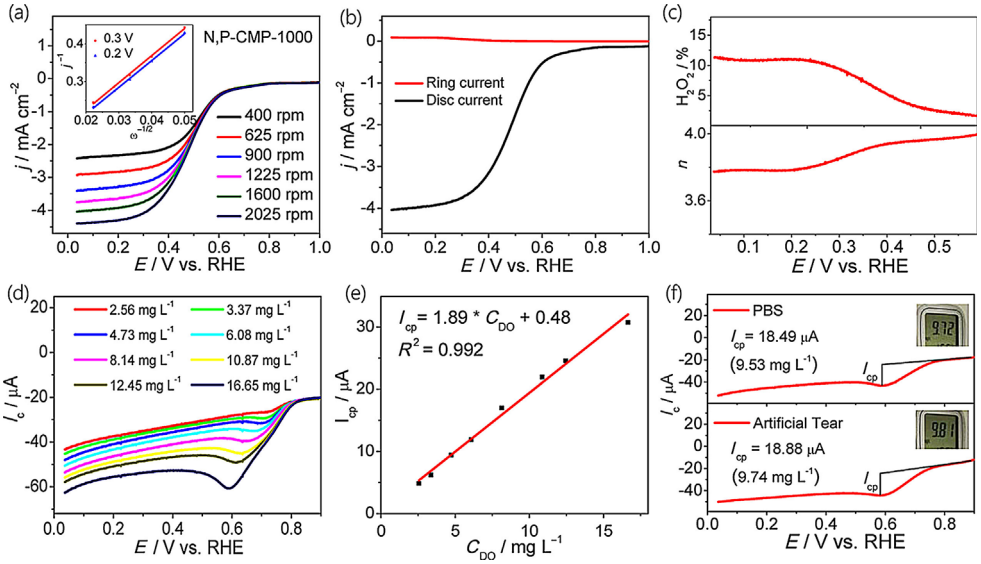

Figure 4. Electrocatalytic activity for ORR and electrochemical DO biosensor performance of N,P-CMP-1000 in 0.01 M PBS solution. (a) LSV curves at different rotating speeds, inset: *K-L* plot at 0.2 and 0.3 V. (b) RRDE measurement of N,P-CMP-1000 at 1600 rpm. (c) Percentage of H_2O_2 in the total ORR products and the electron transfer number per oxygen (*n*) based on the RRDE measurements. (d) LSV curves of N,P-CMP-1000 in PBS solutions with different concentration of dissolved oxygen. (e) Calibration plot of cathodic peak current (I_{cp}) versus concentration of DO (C_{DO}). (f) LSV curves of air-saturated PBS solution (upper) and artificial tear (down). Inset: DO concentrations of the same solutions tested by commercial electrochemical DO sensor (JPB-70A, Qiwei Instrument, China).

ocular biocompatibility of N,P-CMP-1000. Since no electrocatalyst materials will directly enter into the eyeball, the cytotoxicity of N,P-CMP-1000 extract to human corneal epithelial cells (HCEC) could represent a real situation for the wearing DO biosensor. Therefore, a CCK-8 Assay and Live/Dead Cell Double Staining Assay were utilized to determine in vitro cytotoxicity of N,P-CMP-1000 extract to HCEC. The CCK-8 Assay is one of the popular techniques for evaluating in vitro cell viability. N,P-CMP-1000 extraction solutions (or extracts) were prepared by dipping a N,P-CMP-1000 sample in cell culture media for 24 and 48 h, respectively, and an extract (0 h) containing no sample was treated as a negative control (NC). As shown in Figure 5a, HCEC cell survival rates are all higher than 95%,

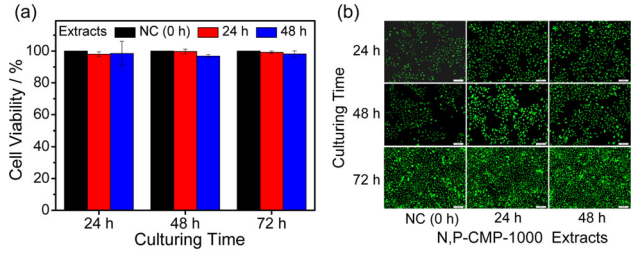

Figure 5. In vitro cytotoxicity of N,P-CMP-1000 extracts against HCEC cells determined by CCK-8 Assay (a) and Live/Dead Cell Double Staining Assay (b).

while cocultured for 24, 48, and 72 h with different N,P-CMP-1000 extracts (0, 24, and 48 h). The results of cell viability by CCK-8 clearly indicate high biocompatibility of N,P-CMP-1000 extracts to HCEC. Live/Dead Cell Double Staining Assay is another simple and direct technique to evaluate in vitro cytotoxicity of N,P-CMP-1000 extracts to HCEC. As shown in Figure 5b, live cells (green) are dominant and dead cells (red) are negligible both in control (NC) and N,P-CMP-1000 extracts (24 and 48 h). Good cell adhesion and growth were also observed as HCEC incubated with different N,P-CMP-1000 extracts. Thus, results from the CCK-8 Assay and Live/Dead Cell Double Staining Assay both indicate good biocompatibility of N,P-CMP-1000 to HCEC cells, encouraging its potential application in eye-wearable biosensors to monitor oxygen concentration in tears.

Conclusions

In summary, we have developed a facile, but effective, method for the synthesis of conjugated microporous polymer (CMP) by acid-catalyzed condensation of commercially available 1,2,4,5-benzenetetramine and hexaketocyclohexane, followed by carbonization in the presence of phytic acid to produce microporous N,P-codoped carbon nanosheets (e.g., N,P-CMP-1000). The resultant N,P-CMP-1000, with an ultrahigh specific surface area, good porosity, and low charge-transfer resistance was demonstrated to be an effective metal-free electrocatalyst for oxygen reduction reaction (ORR) over the whole pH range (i.e., alkaline, acidic, and neutral solutions), exhibiting superior electrocatalytic activity for ORR with a low overpotential, high current density, and good stability. Furthermore, we have, for the first time, demonstrated the potential use of N,P-CMP-1000 as an efficient and biocompatible metal-free ORR catalyst in wearable biosensors with a high sensitivity for detecting dissolved oxygen in tears or other bodily fluids.

Experimental Section

Synthesis of N,P-CMP-900 and N,P-CMP-1000: The CMP-phytic acid composite was prepared by mixing CMP and phytic acid (weight ratio of 1:1) under sonication for 30 min and subsequent freeze-drying. The as-prepared CMP-phytic acid composite was pyrolyzed at 600 °C and 900 °C (or 1000 °C), respectively, for 1 h with a ramp of 5 °C min^{-1} under argon to produce N,P-CMP-900 and N,P-CMP-1000.

Sample characterization: Fourier transform infrared spectra (FTIR) were recorded on a PerkinElmer Spectrum Two IR Spectrometer. Transmission electron microscopy (TEM) and elemental mapping were tested on a FEI Tecnai F20. N_2 adsorption/desorption isotherms were measured at 77 K with a Micromeritics ASAP 2020. Raman spectra were measured using a Renishaw Raman spectrometer using a 514 nm laser. X-ray diffraction (XRD) was conducted on a Rigaku Miniflex II Desktop X-ray diffractometer. X-ray photoelectron spectroscopy (XPS) measurements were performed on a PHI Versaprobe 5000 Scanning X-Ray Photoelectron Spectrometer using a monochromic Al X-ray source (97.9 W, 93.9 eV).

Electrochemical measurements: All electrochemical measurements were performed on CHI 760D electrochemical workstation (CH Instrument, USA) with a typical three-electrode cell using Pt wire as counter electrode and a saturated calomel electrode (SCE) in alkaline solution (or Ag/AgCl in acidic and neutral solutions) as reference electrode. To exclude the potential contamination of the working electrode with dissolved/redeposited platinum in the electrochemical test, a comparison experiment was conducted using both Pt wire and graphite rod as counter electrode and the CV and LSV results clearly showed there was no obvious difference between these two counter electrodes (Figure S14). The electrocatalytic activity towards ORR was evaluated by performing cyclic voltammetry (CV) on glassy carbon electrode and linear sweep voltammetry (LSV) on rotating disk electrode (RDE) and rotating ring-disk electrode (RRDE). The measured potentials were converted to potentials versus RHE ($E_{vsRHE} = E_{vsSCE} + E^{o}_{SCE} + 0.059 \times pH$ or $E_{vs\ RHE} = E_{vsAg/AgCl} + E^{o}_{Ag/AgCl} + 0.059 \times pH$). To prepare the working electrode, 5 mg of a specific sample was dispersed in mixed solution (0.95 mL IPA and 0.05 mL of 5% Nafion aqueous solution) under sonication for 30 min, then 8 μL of the obtained homogeneous catalyst ink was dropped onto a glassy carbon electrode (GCE) and 20 μL on RDE or RRDE electrodes. A Pt/C (20% Pt on Vulcan XC-72R, E-TEK) working electrode was prepared by using the same procedure. 0.1 M $HClO_4$, 0.1 M KOH, and 0.01 M PBS aqueous solutions saturated with nitrogen or oxygen were employed as acidic, alkaline, and neutral electrolyte, respectively.

Acknowledgements

The authors are very grateful for the financial support from the National Natural Science Foundation of China (51433005), the National "Thousand Talents Program" of China, and Case Western Reserve University-Wenzhou Medical University (CON115346).

Conflict of interest

The authors declare no conflict of interest.

Keywords: DO biosensor · energy conversion · metal-free electrocatalyst · N,P-codoped · ORR

[1] a) L. Dai, Y. Xue, L. Qu, H. J. Choi, J. B. Baek, *Chem. Rev.* **2015**, *115*, 4823 – 4892; b) G. Wu, P. Zelenay, *Acc. Chem. Res.* **2013**, *46*, 1878 – 1889; c) C. Hu, L. Dai, *Angew. Chem. Int. Ed.* **2016**, *55*, 11736 – 11758; *Angew. Chem.* **2016**, *128*, 11910 – 11933; d) J. Zhang, Z. Xia, L. Dai, *Sci. Adv.* **2015**, *1*, e1500564.

[2] A. Rahim, *Sens. Actuators B* **2013**, *177*, 231 – 238.

[3] a) M. Gorbet, R. Peterson, D. Mccanna, C. Woods, L. Jones, D. Fonn, *Curr. Eye Res.* **2014**, *39*, 245 – 256; b) J. Hong, T. Qian, Y. Yang, C. Jiang, Z. Liu, X. Sun, S. X. Deng, J. Xu, *Optom. Vision Sci.* **2014**, *91*, 1455 – 1461.

[4] J. Wang, *Electroanalysis* **2005**, *17*, 7 – 14.

[5] J. Wu, H. Yang, *Acc. Chem. Res.* **2013**, *46*, 1848 – 1857.

[6] G. Wu, K. L. More, C. M. Johnston, P. Zelenay, *Science* **2011**, *332*, 443.

[7] a) K. Gong, F. Du, Z. Xia, M. Durstock, L. Dai, *Science* **2009**, *323*, 760 – 764; b) R. Liu, D. Wu, X. Feng, K. Müllen, *Angewandte. Chem. Int. Ed.* **2010**, *49*, 2565 – 2569; *Angew. Chem.* **2010**, *122*, 2619 – 2623; c) Y. Zhao, C. Hu, Y. Hu, H. Cheng, P. G. Shi, L. Qu, *Angew. Chem. Int. Ed.* **2012**, *51*, 11371 – 11375; *Angew. Chem.* **2012**, *124*, 11533 – 11537.

[8] a) L. Qu, Y. Liu, J. B. Baek, L. Dai, *ACS Nano* **2010**, *4*, 1321 – 1326; b) I. Y. Jeon, H. J. Choi, S. M. Jung, J. M. Seo, M. J. Kim, L. Dai, J. B. Baek, *J. Am. Chem. Soc.* **2013**, *135*, 1386 – 1393.

[9] a) D. Yu, Q. Zhang, L. Dai, *J. Am. Chem. Soc.* **2010**, *132*, 15127 – 15129; b) L. Yang, S. Jiang, Y. Zhao, L. Zhu, S. Chen, X. Wang, Q. Wu, J. Ma, Y. Ma, Z. Hu, *Angewandte. Chem. Int. Ed.* **2011**, *50*, 7132 – 7135; *Angew. Chem.* **2011**, *123*, 7270 – 7273; c) S. Wang, D. Yu, L. Dai, *J. Am. Chem. Soc.* **2011**, *133*, 5182 – 5185.

[10] a) J. Zhang, Z. Zhao, Z. Xia, L. Dai, *Nat. Nanotechnol.* **2015**, *10*, 444 – 452; b) C. Hu, L. Dai, *Adv. Mater.* **2017**, *29*, 1604942.

[11] H. Kim, K. Lee, S. I. Woo, Y. Jung, *Phys. Chem. Chem. Phys.* **2011**, *13*, 17505 – 17510.

[12] a) Y. Li, Y. Zhao, H. Cheng, Y. Hu, G. Shi, L. Dai, L. Qu, *J. Am. Chem. Soc.* **2012**, *134*, 15 – 18; b) H. Jin, H. Huang, Y. He, X. Feng, S. Wang, L. Dai, J. Wang, *J. Am. Chem. Soc.* **2015**, *137*, 7588 – 7591.

[13] a) Z. Zhao, M. Li, L. Zhang, L. Dai, Z. Xia, *Adv. Mater.* **2015**, *27*, 6834 – 6840; b) J. Zhang, L. Dai, *Acs Catal.* **2015**, *5*, 7244 – 7253; c) Y. Zheng, Y. Jiao, S. Z. Qiao, *Adv. Mater.* **2015**, *27*, 5372 – 5378.

[14] a) S. Wang, E. Iyyamperumal, A. Roy, Y. Xue, D. Yu, L. Dai, *Angew. Chem. Int. Ed.* **2011**, *50*, 11756 – 11760; *Angew. Chem.* **2011**, *123*, 11960 – 11964; b) S. Wang, L. Zhang, Z. Xia, A. Roy, D. W. Chang, J. B. Baek, L. Dai, *Angew. Chem. Int. Ed.* **2012**, *51*, 4209 – 4212; *Angew. Chem.* **2012**, *124*, 4285 – 4288; c) Y. Zheng, Y. Jiao, L. Ge, M. Jaroniec, S. Z. Qiao, *Angew. Chem. Int. Ed.* **2013**, *52*, 3110 – 3116; *Angew. Chem.* **2013**, *125*, 3192 – 3198; d) Y. Xue, D. Yu, L. Dai, R. Wang, D. Li, A. Roy, F. Lu, H. Chen, Y. Liu, J. Qu, *Phys. Chem. Chem. Phys.* **2013**, *15*, 12220 – 12226.

[15] a) P. A. Denis, C. P. Huelmo, F. Iribarne, *Comput. Theor. Chem.* **2014**, *1049*, 13 – 19; b) K. Qu, Y. Zheng, S. Dai, S. Z. Qiao, *Nano Energy* **2016**, *19*, 373 – 381.

[16] a) J. Zhang, L. Qu, G. Shi, J. Liu, J. Chen, L. Dai, *Angew. Chem. Int. Ed.* **2016**, *55*, 2230 – 2234; *Angew. Chem.* **2016**, *128*, 2270 – 2274; b) M. Borghei, N. Laocharoen, E. Kibena-Põldsepp, L. S. Johansson, J. Campbell, O. J. Rojas, *Appl. Catal. B* **2017**, *204*, 394 – 402.

[17] a) J. Shui, M. Wang, F. Du, L. Dai, *Sci. Adv.* **2015**, *1*, e1400129; b) J. J. Li, Y. M. Zhang, X. H. Zhang, J. Z. Huang, J. C. H. P. Xu, B. Song, *ACS Appl. Mater. Interfaces* **2017**, *9*, 398 – 405.

[18] Y. R. He, F. Du, Y. X. Huang, L. M. Dai, W. W. Li, H. Q. Yu, *J. Mater. Chem. A* **2016**, *4*, 1632 – 1636.

[19] W. Gu, L. Hu, J. Li, E. Wang, *Acs Appl. Mater. Interfaces* **2016**, *8*, 35281 – 35288.

[20] a) D. S. Yang, D. Bhattacharjya, S. Inamdar, J. Park, J. S. Yu, *J. Am. Chem. Soc.* **2012**, *134*, 16127 – 16130; b) J. Liang, X. Du, C. Gibson, X. W. Du, S. Z. Qiao, *Adv. Mater.* **2013**, *25*, 6150; c) W. Wei, H. Liang, K. Parvez, X. Zhuang, X. Feng, K. Müllen, *Angew. Chem. Int. Ed.* **2014**, *53*, 1570 – 1574; *Angew. Chem.* **2014**, *126*, 1596 – 1600.

[21] a) Y. Wan, D. Zhao, *Chem. Rev.* **2007**, *107*, 2821 – 2856; b) J. Liu, N. P. Wickramaratne, S. Z. Qiao, M. Jaroniec, *Nat. Mater.* **2015**, *14*, 763 – 774.

[22] a) L. Huang, Z. Xiang, D. Cao, *J. Mater. Chem. A* **2013**, *1*, 3851 – 3855; b) A. P. Côté, A. I. Benin, N. W. Ockwig, M. O'Keeffe, A. J. Matzger, O. M. Yaghi, *Science* **2005**, *310*, 1166 – 1170; c) R. Dawson, A. I. Cooper, D. J. Adams, *Prog. Polym. Sci.* **2012**, *37*, 530 – 563.

[23] Z. Xiang, D. Cao, L. Huang, J. Shui, M. Wang, L. Dai, *Adv. Mater.* **2014**, *26*, 3315 – 3320.

[24] a) Y. Kou, Y. Xu, Z. Guo, D. Jiang, *Angew. Chem. Int. Ed.* **2011**, *50*, 8753 – 8757; *Angew. Chem.* **2011**, *123*, 8912 – 8916; b) C. Gu, N. Huang, Y. Chen, L. Qin, H. Xu, S. Zhang, F. Li, Y. Ma, D. Jiang, *Angew. Chem. Int. Ed.* **2015**, *54*, 13594 – 13598; *Angew. Chem.* **2015**, *127*, 13798 – 13802.

[25] J. Mahmood, E. K. Lee, M. Jung, D. Shin, I. Y. Jeon, S. M. Jung, H. J. Choi, J. M. Seo, S. Y. Bae, S. D. Sohn, N. Park, J. H. Oh, H. J. Shin, J. B. Baek, *Nat. Commun.* **2015**, *6*, 6486.

[26] L. Lin, Q. Zhu, A. W. Xu, *J. Am. Chem. Soc.* **2014**, *136*, 11027 – 11033.

[27] Z. Huang, H. Zhou, W. Yang, C. Fu, L. Chen, Y. Kuang, *ChemCatChem* **2017**, *9*, 987 – 996.

[28] Y. Xu, X. Lin, *Electrochim. Acta* **2007**, *52*, 5140 – 5149.

[29] M. S. El-Deab, T. Ohsaka, *Electrochem. Commun.* **2002**, *4*, 288 – 292.

[30] S. M. Silva, L. F. Aguiar, R. M. S. Carvalho, A. A. Tanaka, F. S. Damos, R. C. S. Luz, *Microchim. Acta* **2016**, *183*, 1251 – 1259.

Manuscript received: April 23, 2018
Version of record online: ■■ ■■, 0000

FULL PAPER

Oxygen Reduction Reaction

D. Lin, C. Hu, H. Chen, J. Qu,* L. Dai**

■■ – ■■

Microporous N,P-Codoped Graphitic Nanosheets as an Efficient Electrocatalyst for Oxygen Reduction in Whole pH Range for Energy Conversion and Biosensing Dissolved Oxygen

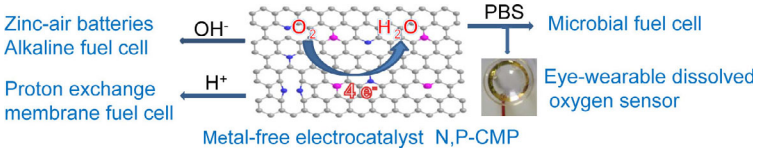

Eye spy: Microporous N,P-codoped carbon nanosheets were prepared by acid-catalyzed condensation of commercially available 1,2,4,5-benzenetetramine and hexaketocyclohexane, followed by carbonization in the presence of phytic acid, which were used as efficient metal-free electrocatalysts for ORR over whole pH range (i.e., alkaline solution, acidic and neutral solutions), and eye-wearable biosensors for sensing dissolved oxygen in tears or other body fluids.